Comparative Preclinical Biodistribution, Dosimetry, and Endoradiotherapy in Metastatic Castration-Resistant Prostate Cancer Using ^{19}F/^{177}Lu-rhPSMA-7.3 and ^{177}Lu-PSMA I&T

Nahid Yusufi[1], Alexander Wurzer[2], Michael Herz[1], Calogero D'Alessandria[1], Benedikt Feuerecker[1], Wolfgang Weber[1], Hans-Jürgen Wester[2], Stephan Nekolla*[1], and Matthias Eiber*[1]

[1]*Department of Nuclear Medicine, Klinikum rechts der Isar, Technical University of Munich, Munich, Germany; and* [2]*Chair for Pharmaceutical Radiochemistry, Technical University of Munich, Garching, Germany*

Radiohybrid prostate-specific membrane antigen (rhPSMA) ligands are applicable as radiochemical twins for both diagnostic PET imaging and endoradiotherapy. On the basis of preliminary data as a diagnostic ligand, the isomer rhPSMA-7.3 is a promising candidate for potential endoradiotherapy. The aim of this preclinical evaluation was to assess the biodistribution, dosimetry, and therapeutic efficacy of ^{19}F/^{177}Lu-rhPSMA-7.3 in comparison to the established therapeutic agent ^{177}Lu-PSMA I&T (imaging and therapy). **Methods:** The biodistribution of ^{19}F/^{177}Lu-rhPSMA-7.3 and ^{177}Lu-PSMA I&T was determined in LNCaP tumor–bearing severe combined immunodeficiency (SCID) mice after sacrifice at defined time points up to 7 d (n = 5). Organs and tumors were dissected, percentage injected dose per gram (%ID/g) was determined, and dosimetry was calculated using OLINDA/EXM, version 1.0. The therapeutic efficacy of a single 30-MBq dose of ^{19}F/^{177}Lu-rhPSMA-7.3 (n = 7) was compared with that of ^{177}Lu-PSMA I&T in treatment groups (n = 7) and control groups (n = 6–7) using C4-2 tumor–bearing SCID mice by evaluating tumor growth and survival over 6 wk after treatment. **Results:** The biodistribution of ^{19}F/^{177}Lu-rhPSMA-7.3 revealed fast blood clearance (0.63 %ID/g at 1 h after injection), and the highest activity uptake was in the spleen and kidneys, particularly in the first hour (33.25 %ID/g and 207.6 %ID/g, respectively, at 1 h after injection), indicating a renal excretion pathway. Compared with ^{177}Lu-PSMA I&T, ^{19}F/^{177}Lu-rhPSMA-7.3 exhibited an initial (1 h) 2.6-fold higher tumor uptake in LNCaP xenografts and a longer retention (4.5 %ID/g vs. 0.9 %ID/g at 168 h). The tumor dose of ^{19}F/^{177}Lu-rhPSMA-7.3 was substantially higher (e.g., 7.47 vs. 1.96 μGy/MBq at 200 mm^3) than that of ^{177}Lu-PSMA I&T. In most organs, absorbed doses were higher for ^{177}Lu-PSMA I&T. A significantly greater tumor size reduction was shown for a single dose of ^{19}F/^{177}Lu-rhPSMA-7.3 than for ^{177}Lu-PSMA I&T at the end of the experiment (P = 0.0167). At the predefined termination of the experiment at 6 wk, 7 of 7 and 3 of 7 mice were still alive in the ^{19}F/^{177}Lu-rhPSMA-7.3 and ^{177}Lu-PSMA I&T groups, respectively, compared with the respective control groups, with 0 of 7 and 0 of 6 mice. **Conclusion:** Compared with ^{177}Lu-PSMA I&T, ^{19}F/^{177}Lu-rhPSMA-7.3 can be considered a suitable candidate for clinical translation because it has similar clearance kinetics and a similar radiation dose to healthy organs but superior tumor uptake and retention. Preliminary treatment experiments showed a favorable antitumor response.

Key Words: PSMA; prostate cancer; ^{177}Lu-radioligand therapy; preclinical biodistribution, dosimetry

J Nucl Med 2021; 62:1106–1111
DOI: 10.2967/jnumed.120.254516

In the last 2 decades, prostate-specific membrane antigen (PSMA)–targeting radiopharmaceuticals have been extensively investigated for diagnosis and treatment of prostate cancer. Several small-molecule inhibitors are in different stages of clinical development. ^{68}Ga-PSMA-11 is the most widely used PSMA ligand for diagnostics. PSMA-617 and PSMA I&T (imaging and therapy) dominate the field of PSMA endoradiotherapy (*1–4*). Most recently published clinical phase II data indicate that patients with metastatic castration-resistant prostate cancer for whom only limited therapeutic options are currently available can benefit from combined PSMA-targeted diagnosis and ^{177}Lu-PSMA endoradiotherapy (*5*).

Recently, the new concept of radiohybrid PSMA (rhPSMA) ligands was introduced (*6*). These ligands are considered fully theranostic agents because they can be labeled with both diagnostic and therapeutic radiometals and with ^{18}F. ^{18}F inherits several advantages for imaging, such as a long half-life, enhanced image resolution, and large-scale production throughout centers using cyclotrons (*7*). Furthermore, the use of radiochemical twins (e.g., ^{18}F/^{nat}Lu-rhPSMA or ^{19}F/^{177}Lu-rhPSMA) allows pretherapeutic PET-based imaging and dosimetry, whereas the ^{177}Lu-labeled counterpart is used for endoradiotherapy (Fig. 1) (*8*).

In the first clinical retrospective reports, promising results for biodistribution, image quality, and tumor uptake using the ^{18}F-labeled lead compound rhPSMA-7 have been reported. Additional data indicated high diagnostic performance for detection of lymph node metastases in primary prostate cancer and localization of biochemical recurrence (*9–11*). Most recently, the different isomers (7.1, 7.2, 7.3, and 7.4) of its lead compound, rhPSMA-7, have been analyzed separately in preclinical studies (*12*). The single isomer rhPSMA-7.3 is regarded as the most promising candidate for ^{18}F-based imaging, and a phase I study (ClinicalTrials.gov identifier NCT03995888) for assessing biodistribution and internal dosimetry in healthy individuals and in prostate cancer patients has recently been completed. The diagnostic performance of rhPSMA-7.3 in newly diagnosed prostate cancer or suspected recurrence is being investigated in 2 multicenter phase III studies (NCT04186819 and NCT04186845).

The aim of this preclinical evaluation was to investigate the potential of ^{19}F/^{177}Lu-rhPSMA-7.3 for PSMA radioligand therapy by

Received Aug. 10, 2020; revision accepted Dec. 4, 2020.
For correspondence or reprints, contact Matthias Eiber (matthias.eiber@tum.de).
*Contributed equally to this work.

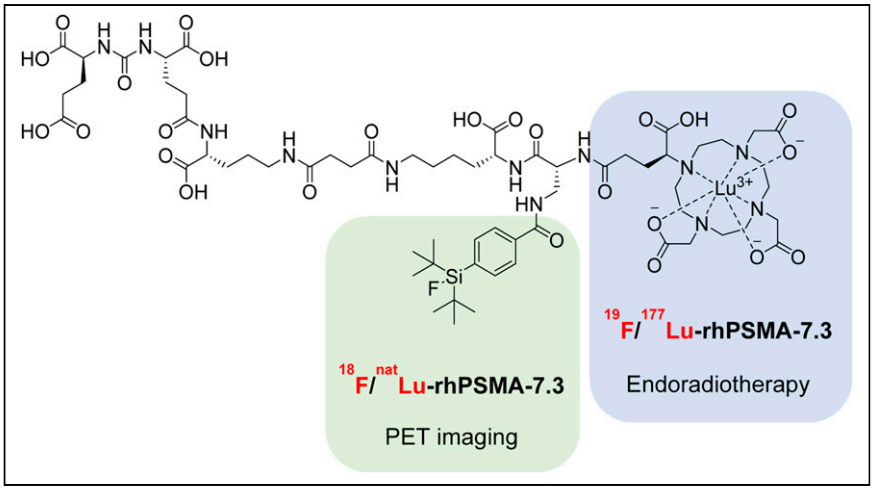

FIGURE 1. Radiohybrid concept of radiochemical twins ^{18}F/^{nat}Lu-rhPSMA-7.3 and ^{19}F/^{177}Lu-rhPSMA-7.3. ^{18}F labeling at silicon-fluoride-acceptor (SiFA) binding site (green)—whereas ^{nat}Lu is chelated—allows PET-based imaging. rhPSMA-7.3 chelated with ^{177}Lu (blue) and binding of nonradioactive ^{19}F is used for endoradiotherapy.

direct comparison to ^{177}Lu-PSMA I&T as an established agent for clinical endoradiotherapy (*3*,*8*,*13*). We used established xenograft mouse models and explored longitudinal biodistribution, dosimetry, and therapeutic effect in a proof-of-concept study of both ligands.

MATERIALS AND METHODS

Mice

All animal experiments were approved by local authorities (animal license 55.2-1-54-2532-216-2015) and handled according to guidelines for the welfare and use of animals in cancer research experimentation. Male severe combined immunodeficiency (SCID CB17/Icr-Prkdc^{scid}/IcrIcoCrl) mice at least 6 wk old were used for all studies.

Cell Culture and Tumor Implantation

LNCaP and C4-2 cell lines (kind gift of George Thalmann, University of Bern, Switzerland) were used in the tumor xenograft studies to assess the tumor uptake and therapeutic effect of the assessed radioligands, respectively. C4-2 are isolated cells from a subcutaneous LNCaP xenograft tumor of a castrated mouse and reflect androgen-independent disease (*14*). The cell lines were cultivated in RPMI medium supplemented with 10% fetal calf serum and penicillin–streptomycin (100 IU/mL) at 37°C in a 5% CO_2/humidified air atmosphere. For subcutaneous inoculation, the animals were anesthetized with 3%–5% (v/v) isoflurane inhalation, and 5×10^6 cells in 100 μL of serum-free RPMI medium and 100 μL of Matrigel (Corning) were injected into the right shoulder region.

Synthesis of ^{19}F/^{177}Lu-rhPSMA-7.3 and ^{177}Lu-PSMA I&T

To produce the ^{19}F/^{177}Lu-rhPSMA-7.3, 1.5 GBq of carrier-added $^{177}LuCl_3$ (IDB Holland B.V.) were added to 50 nmol of the uncomplexed precursor. The solution was incubated in NaOAc (0.4 M, 400 μL, pH 5.5) and in 4 mg of gentisic acid at 90°C for 30 min (radiochemical purity, 98%–99%).

The ^{177}Lu-PSMA I&T was synthesized on a GRP synthesis module (Scintomics). In brief, 200 μg of the PSMA I&T precursor in 50% (v/v) EtOH/H_2O was labeled with 10 GBq of carrier-added $^{177}LuCl_3$ (IDB Holland B.V.) in NaOAc (0.04 M, pH 5.5) at 90°C for 30 min, with subsequent addition of 4 mg of gentisic acid to prevent radiolysis (radiochemical purity, 99%–100%).

Biodistribution

Approximately 40 pmol of ^{19}F/^{177}Lu-rhPSMA-7.3 (molar activity, 30 MBq/nmol) and ^{177}Lu-PSMA I&T (molar activity, 75 MBq/nmol) in 200 μL of phosphate-buffered saline were injected intravenously into the tail vein of LNCaP xenograft SCIDs for biodistribution studies ($n = 5$ per time point). The animals were sacrificed at the defined time points (1, 12, 24, 48, and 168 h after injection). Blood and tissues of interest, including tumor, were collected, weighed, and counted using an automated γ-counter (2480 Wizard2; PerkinElmer). Tumor-to-kidney uptake ratios were calculated, since the kidneys are one of the dose-limiting organs in clinical PSMA-directed endoradiotherapy.

Radioligand Therapy Using ^{19}F/^{177}Lu-rhPSMA-7.3 or ^{177}Lu-PSMA I&T

For endoradiotherapy studies applying ^{19}F/^{177}Lu-rhPSMA-7.3 or ^{177}Lu-PSMA I&T, C4-2 xenograft–bearing SCIDs ($n = 6$–7) were injected with a single dose of 30 MBq in 200 μL of phosphate-buffered saline (molar activity, 30 MBq/nmol). In the respective control groups, animals were injected with 1 nmol of nonradioactive rhPSMA-7.3 or PSMA I&T. PSMA expression in the xenografts was determined by pretherapeutic PET imaging 1 h after injection of ^{18}F/^{nat}Ga-rhPSMA-7.3 on the third day before therapy. Tumor size was measured once weekly by MRI until 6 wk after injection. Tumor volumes at baseline (3 wk after inoculation and 5 d before treatment) did not significantly differ, with a mean of 147.5 ± 7.3 mm^3, 122.8 ± 38.2 mm^3, 195.0 ± 41.4 mm^3, and 275.8 ± 113.6 mm^3 ($P = 0.2550$) for ^{19}F/^{177}Lu-rhPSMA-7.3, rhPSMA-7.3, ^{177}Lu-PSMA I&T, and PSMA I&T, respectively. Endpoint criteria were defined as tumor size exceeding 1.5 cm or critical scoring of an animal's well-being. Predefined termination of the experiment by the animal experiment license was at 6 wk.

MRI

Therapeutic effects on tumor size in xenograft animals were monitored on a small-animal 7-T preclinical MR scanner (Agilent/GE Healthcare magnet, Bruker Avance III HD electronics with ParaVision, version 6.0.1). The animals were anesthetized with 5% (v/v) isoflurane inhalation and were maintained at 1.5%–3% (v/v) during scanning. T2-weighted turbo RARE (rapid acquisition with relaxation enhancement) images were acquired in axial orientation, with an echo time of 40 ms, a repetition time of 3.6 s, a RARE factor of 4, 4 averages, a 180 × 180 matrix, a 36 × 36 mm field of view, 31 slices, a slice thickness of 1 mm, fat saturation, a receiver bandwidth of 100 kHz, and a total acquisition time of 3 min 36 s. DICOM files from T2-weighted MR scans were analyzed in a RadiAnt DICOM viewer, version 5.0.2. The dimensions of the ellipsoid-shaped tumors were measured on coronal and axial images. Tumor volumes were calculated using the following formula: volume = $4/3 \times \pi \times a \times b \times c$ (a/b/c = semiaxes).

Dosimetry Calculations

Five time points were used to calculate the time-integrated activity coefficients. The time integrals of activity for the accumulation in the significant source organs were generated both with numeric integration and with physical decay, according to the method of Yuan (*15*). Normal-organ radiation doses were estimated for the 70-kg standard adult anatomic model using the time-dependent organ activity accumulation (in percentage injected dose per gram, %ID/g) and the total-body activities measured in the biodistribution studies on mice (*16*,*17*).

Activity accumulations in mice were converted to tissue fractional activities in the 70-kg standard adult using the relative fractional organ masses in the standard adult and the standard 25-g mouse. Time-integrated activity coefficients were calculated by numeric integration using the trapezoidal rule and the rest of the body. ^{177}Lu residence times were calculated as the difference between the total-body residence time and the sum of the organ and urine residence times. Finally, absorbed doses (in mGy/MBq) in the organs of a standard adult were calculated using OLINDA/EXM, version 1.0, according to Stabin et al. (*18*).

For estimating tumor doses, the unit density sphere model described by Stabin et al. (*19*) was used. Therefore, the values for the total number of decays in MBq × h/MBq units based on the biodistribution data were inputted into OLINDA/EXM.

Statistics

Data are presented as mean ± SD or SEM. Mann–Whitney testing was performed to compare different groups. Survival was analyzed by the Kaplan–Meyer method and log-rank (Mantel–Cox) testing. Statistical significance was considered present at a P value of less than 0.05. Prism (version 5.04, GraphPad Software, Inc.) was used for all statistical analyses.

RESULTS

Biodistribution and Tumor Uptake of ^{19}F/^{177}Lu-rhPSMA-7.3 and ^{177}Lu-PSMA I&T

^{19}F/^{177}Lu-rhPSMA-7.3 showed the typical biodistribution pattern of PSMA-targeting ligands, with fast blood clearance, low uptake in normal organs, except for kidneys and spleen, and an overall continuous decrease over 7 d (Fig. 2A). Uptake in the kidneys and spleen was high for both ligands, with initially higher numbers for ^{19}F/^{177}Lu-rhPSMA-7.3 (207.59 ± 30.98 %ID/g and 33.25 ± 8.62 %ID/g, respectively) than for ^{177}Lu-PSMA I&T (165.50 ± 20.46 %ID/g and 26.06 ± 18.99 %ID/g, respectively) at 1 h (Figs. 2A and 2B; Supplemental Tables 1 and 2; supplemental materials

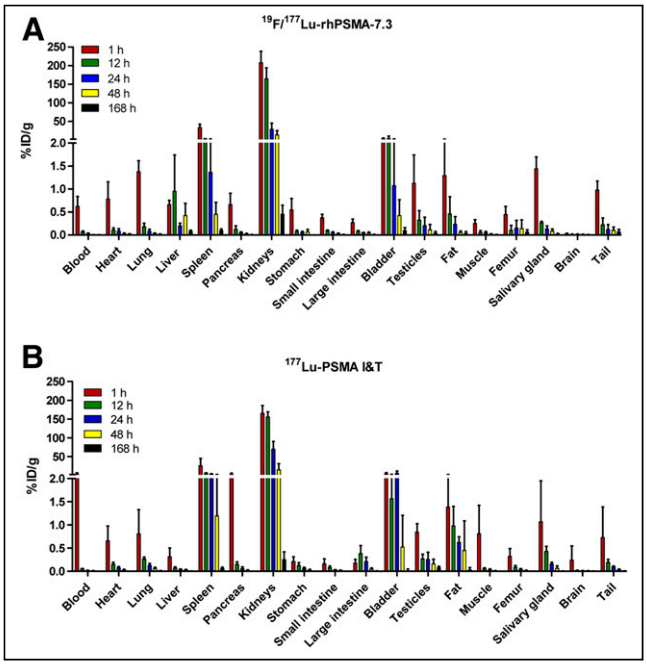

FIGURE 2. Biodistribution of ^{19}F/^{177}Lu-rhPSMA-7.3 (A) and ^{177}Lu-PSMA I&T (B) at 1, 12, 24, 48, and 168 h after intravenous administration of 40 pmol of respective radiopeptide. Mean %ID/g ± SD is shown (n = 5).

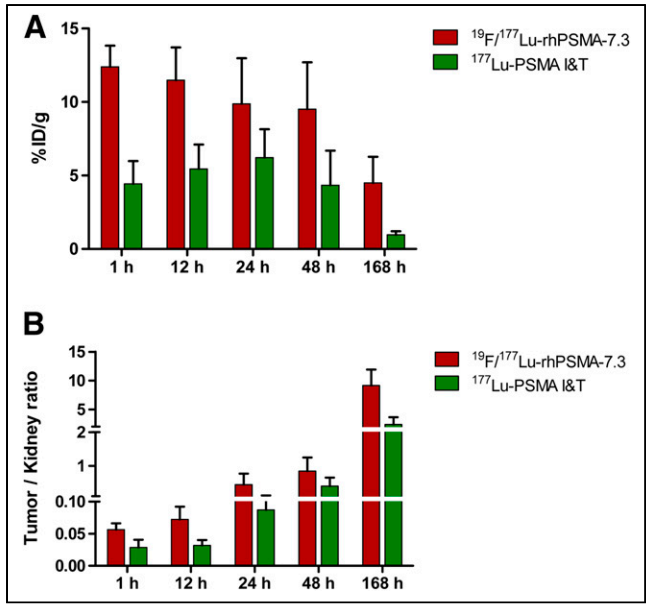

FIGURE 3. Activity uptake in %ID/g of ^{19}F/^{177}Lu-rhPSMA-7.3 and ^{177}Lu-PSMA I&T in LNCaP tumors over 1–168 h (A). Tumor-to-kidney uptake ratios of ^{19}F/^{177}Lu-rhPSMA-7.3 and ^{177}Lu-PSMA I&T in different time groups from 1 to 168 h (B). Data are mean ± SD (n = 5).

are available at http://jnm.snmjournals.org). The decline in these organs over the following days appeared to be faster for ^{19}F/^{177}Lu-rhPSMA-7.3 (35.70 ± 16.63 %ID/g in kidneys and 1.37 ± 1.21 %ID/g in spleen at 24 h) than for ^{177}Lu-PSMA I&T (76.84 ± 22.70 %ID/g in kidneys and 4.02 ± 0.74 %ID/g in spleen at 24 h). At 168 h after injection, only minimal activity was observed in any organ with either radiopharmaceutical.

Tumor uptake in LNCaP xenografts was 2.8-fold higher for ^{19}F/^{177}Lu-rhPSMA-7.3 than for ^{177}Lu-PSMA I&T at 1 h (12.4 ± 1.4 %ID/g vs. 4.4 ± 1.5 %ID/g, respectively) and gradually decreased for ^{19}F/^{177}Lu-rhPSMA-7.3 until the end of the study (Figs. 3A and 3B). Tumor uptake remained higher for ^{19}F/^{177}Lu-rhPSMA-7.3 than for ^{177}Lu-PSMA I&T at all time points, including at 168 h after injection, when a 4.7-fold higher activity retention was seen for ^{19}F/^{177}Lu-rhPSMA-7.3 than for ^{177}Lu-PSMA I&T (4.5 ± 1.8 %ID/g vs. 0.9 ± 0.2 %ID/g). ^{177}Lu-PSMA I&T showed a contrasting kinetic profile of tumor uptake, increasing until 24 h after injection, after which uptake decreased for the remainder of the study. Tumor-to-kidney ratios were on average 2-fold higher in favor of ^{19}F/^{177}Lu-rhPSMA-7.3 at all assessed time points (Fig. 3B; Supplemental Table 3).

Comparison of the kinetics of retention on the logarithmic scale in the kidneys; bone, including marrow; and tumor revealed that clearance was fastest in the kidneys, with a similar trend toward initially higher uptake with ^{19}F/^{177}Lu-rhPSMA-7.3 and similar clearance to ^{177}Lu-PSMA I&T (Fig. 4). Clearance was slower from bone, including marrow, for ^{19}F/^{177}Lu-rhPSMA-7.3. Retention was most prolonged in tumors, with a trend toward greater retention, as well as significantly higher initial uptake, for ^{19}F/^{177}Lu-rhPSMA-7.3.

Radiation Dosimetry

Absorbed doses in major organs and tissues are presented in Figure 5A and Supplemental Tables 4 and 5. Delivered doses to all tissues were higher for ^{177}Lu-PSMA I&T than for ^{19}F/^{177}Lu-rhPSMA-7.3, except in the liver (1.60E−02 vs. 3.22E−03 mGy/

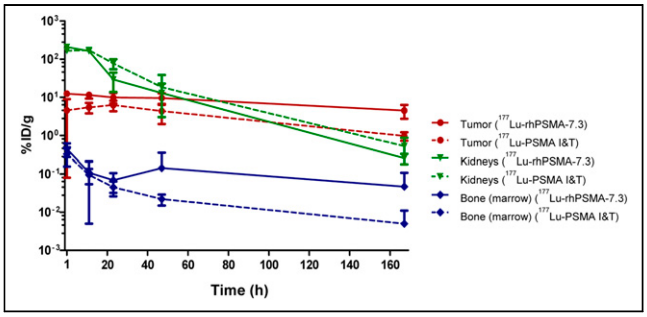

FIGURE 4. Plot of activity accumulation in %ID/g over time (1–168 h) in tumors (LNCaP), kidneys, and bone (marrow) after administration of ^{19}F/^{177}Lu-rhPSMA-7.3 and ^{177}Lu-PSMA I&T. Data are mean ± SD. Clearance rates (in 1/h) for ^{19}F/^{177}Lu-rhPSMA-7.3 vs. ^{177}Lu-PSMA I&T are, respectively, 0.006 vs. 0.012 in tumor, 0.031 vs. 0.035 in kidneys, and 0.006 vs. 0.017 in bone (marrow).

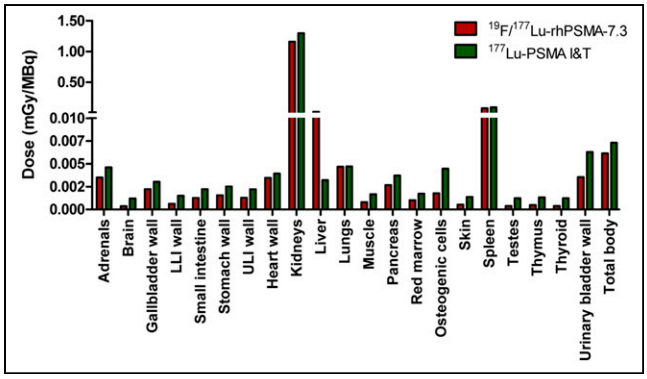

FIGURE 5. Calculated doses in mGy/MBq delivered to human organs and tissues for ^{19}F/^{177}Lu-rhPSMA-7.3 and ^{177}Lu-PSMA I&T.

MBq). Exemplarily, absorbed doses in the kidney and bone marrow as the most relevant organs at risk for endoradiotherapy were 1.16 versus 1.30 mGy/MBq and 1.05E−03 versus 1.76E−03 mGy/MBq for ^{19}F/^{177}Lu-rhPSMA-7.3 versus ^{177}Lu-PSMA I&T, respectively. The differences in absorbed doses were most pronounced in the brain (3.63E−04 vs. 1.21E−03 mGy/MBq), thymus (4.85E−04 vs. 1.33E−03 mGy/MBq), and thyroid (3.92E−04 vs. 1.25E−03 mGy/MBq).

Doses delivered to the tumors are shown in Supplemental Table 6 as a function of the unit density sphere. ^{19}F/^{177}Lu-rhPSMA-7.3 delivered a 2.6-fold higher radiation dose to LNCaP tumors than ^{177}Lu-PSMA I&T did, independent of the tumor size (e.g., 9.90E02 vs. 3.78E02 mGy/MBq at a tumor volume of 1 mL).

Proof-of-Concept Endoradiotherapy

Changes in absolute tumor volumes and in relative tumor volumes in all groups over time are presented in Figure 6, Supplemental Figure 1, and Supplemental Table 7. Overall survival in all treatment groups is shown in Supplemental Figure 2. Tumors continued to grow in the control groups after application of unlabeled rhPSMA-7.3 and PSMA I&T. Median survival as determined by the endpoint of tumors larger than 1.5 cm was 14 d for unlabeled rhPSMA-7.3 and 10.5 d for PSMA I&T.

Both tumors treated with ^{19}F/^{177}Lu-rhPSMA-7.3 and tumors treated with ^{177}Lu-PSMA I&T showed growth retention. However, tumors in the ^{177}Lu-PSMA I&T group showed earlier regrowth after initial retention than did the ^{19}F/^{177}Lu-rhPSMA-7.3 group. By the end of the study (week 6), tumors treated with ^{19}F/^{177}Lu-rhPSMA-7.3 were significantly smaller than those treated with ^{177}Lu-PSMA I&T (absolute volumes, 170.3 ± 46.1 mm^3 vs. 712.2 ± 119.4 mm^3; relative change, 1.2 ± 0.3 mm^3 vs. 6.2 ± 2.7, $P = 0.0167$). The median survival of ^{177}Lu-PSMA I&T–treated animals was 35 d, whereas all mice treated with ^{19}F/^{177}Lu-rhPSMA-7.3 had prolonged survival up to the end of the treatment study (week 6).

DISCUSSION

The aim of these preclinical studies was to investigate the pharmacokinetics, dosimetry, and therapeutic efficacy of the novel theranostic agent ^{19}F/^{177}Lu-rhPSMA-7.3 in comparison to the clinically established agent ^{177}Lu-PSMA I&T. The biodistribution pattern of ^{177}Lu-PSMA I&T was consistent with previously published preclinical data (*20*,*21*). A similar uptake profile in healthy organs was found for ^{19}F/^{177}Lu-rhPSMA-7.3 over the assessment period of 7 d. However, compared with ^{177}Lu-PSMA I&T, ^{19}F/^{177}Lu-rhPSMA-7.3 seemed to have faster binding and a similar clearance kinetic from healthy tissues as demonstrated by higher values in organs, the low blood concentration in the first hours, and a subsequent similar decline in most organs. In contrast, whereas a higher amount of ^{177}Lu-PSMA I&T was present in the blood in the first hours, the peaks in uptake and clearance from most healthy organs were delayed. The preclinical biodistribution for ^{19}F/^{177}Lu-rhPSMA-7.3 in this study was similar to clinical data in prostate cancer patients using the ^{18}F-labeled mixed diastereoisomeric compound rhPSMA-7 (*9*).

Our data indicate clear differences in tumor uptake between ^{19}F/^{177}Lu-rhPSMA-7.3 and ^{177}Lu-PSMA I&T in LNCaP xenografts. In our study, tumor uptake was substantially higher for ^{19}F/^{177}Lu-rhPSMA-7.3 than for ^{177}Lu-PSMA I&T at all assessed time points up to 7 d. This finding agrees with recently performed in vitro evaluations by Wurzer et al. of rhPSMA-7 chelated with ^{68}Ga (*6*). The internalization of ^{68}Ga-rhPSMA-7 in LNCaP cells was considerably higher (~125% of reference) than previously found for PSMA I&T chelated with either ^{68}Ga or ^{177}Lu (range, 59%–76% of reference) (*22*). In further in vitro characterization studies of the individual isomers of the rhPSMA-7 lead compound, rhPSMA-7.3 was characterized by a significantly higher internalization rate in LNCaP tumor cells (161.9% of reference; (*12*)). Wurzer et al. also reported improved binding affinities (half-maximal inhibitory concentration) for the rhPSMA-7 isomers compared with KuE-based PSMA inhibitors, of which PSMA I&T is one (*6*).

Given the similar uptake of the two radiopharmaceuticals in the kidneys, the increased accumulation rate of ^{19}F/^{177}Lu-rhPSMA-7.3 in tumor tissue resulted in improved tumor-to-kidney ratios at all assessed time points up to 7 d in comparison with ^{177}Lu-PSMA I&T. This preclinical observation, if preserved in clinical translation, could be a potential advantage of ^{19}F/^{177}Lu-rhPSMA-7.3 over ^{177}Lu-PSMA I&T. Renal toxicity is a major concern in clinical use of PSMA endoradiotherapy (*23*,*24*), although only rare cases of renal toxicity for PSMA endoradiotherapy have been reported and the clinical dosimetry of ^{177}Lu-PSMA-617 and ^{177}Lu-PSMA I&T indicate that a critical dose to the kidneys is reached after 4–6 cycles. Because renal toxicity after radionuclide therapy is often a long-term side effect, this possibility is especially relevant for potential future application of PSMA endoradiotherapy in earlier stages of disease progression. Another potential at-risk organ, bone marrow, also revealed similar absorbed doses with both radiopharmaceuticals. Bone marrow toxicity, grade 3 or

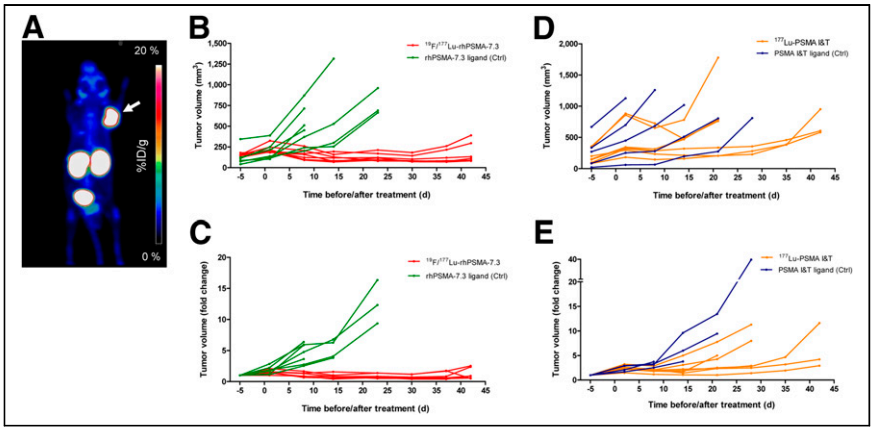

FIGURE 6. (A) Representative pretherapeutic PET image using $^{18}F/^{nat}Ga$-rhPSMA-7.3. C4-2 xenograft is indicated by arrow. (B–E) Tumor growth curves for individual mice in treatment and control groups of endoradiotherapy study on days before or after treatment (day 0).x

4, has been reported in up to one third of patients, especially in patients with diffuse bone marrow involvement (*25*,*26*). Yet bone marrow toxicity in patients with a low bone tumor burden is rare. In summary, improved uptake in tumors at similar uptake in kidneys and bone marrow might indicate that lower radioactive doses of $^{19}F/^{177}Lu$-rhPSMA-7.3 can be administered to achieve treatment effects similar to those of established PSMA-targeting peptides while allowing for more therapy sessions, given the lower dose to organs at risk per cycle.

Notably, salivary gland toxicity is a major concern using α-emitters and β-emitters (*27*,*28*). In our preclinical study, salivary gland uptake was not assessed, given the differences in PSMA expression between murine and human salivary glands (*29*–*32*). This issue has to be investigated either within a phase I clinical trial or using different clinical models (e.g., pigs) as previously published for ^{177}Lu-PSMA 617 (*32*).

Calculations of estimated doses delivered to major human organs and tissues were based on the biodistribution data of $^{19}F/^{177}Lu$-rhPSMA-7.3 and ^{177}Lu-PSMA I&T over 7 d and revealed smaller absorbed doses for $^{19}F/^{177}Lu$-rhPSMA-7.3. Dose calculations using preclinical data for ^{177}Lu-PSMA I&T have already been performed by Weineisen et al., resulting in similar absorbed doses in major organs (*33*). Clinical dosimetry data have been collected both for ^{177}Lu-PSMA I&T and for ^{177}Lu-PSMA-617. Absorbed doses in organs do not substantially differ between the 2 ligands, especially for the known dose-limiting organs kidney and salivary gland (*34*–*39*).

A direct comparison to ^{177}Lu-PSMA-617, which is currently being evaluated in a phase III multicenter trial, was not performed in our study. However, Kuo et al. has evaluated ^{177}Lu-PSMA-617 uptake in LNCaP tumor tissue in the same xenograft animal model and calculated the corresponding delivered dose. At all tumor volumes, ^{177}Lu-PSMA-617 delivered smaller doses than those calculated for ^{177}Lu-PSMA I&T in our study (*40*). Despite differences in methodology, this finding provides some evidence that $^{19}F/^{177}Lu$-rhPSMA-7.3 might also offer enhanced tumor-to-organ characteristics compared with ^{177}Lu-PSMA-617.

In the proof-of concept therapy study, we observed a significantly higher antitumor effect using $^{19}F/^{177}Lu$-rhPSMA-7.3 than using ^{177}Lu-PSMA I&T. By the end of the observation time (week 6), all tumors treated with ^{177}Lu-PSMA I&T were exhibiting clear regrowth compared with $^{19}F/^{177}Lu$-rhPSMA-7.3–treated tumors, which remained similar to the size at baseline. The substantial growth of large tumors in the control groups and in the ^{177}Lu-PSMA I&T group led to experimental termination for these mice. Thus, a clear trend to longer median survival was present for $^{19}F/^{177}Lu$-rhPSMA-7.3. When data from biodistribution and treatment experiments are combined, it can be assumed that improved uptake (%ID/g) and retention, subsequently leading to higher tumor doses, of $^{19}F/^{177}Lu$-rhPSMA-7.3 in tumor tissue have resulted in this prolonged growth inhibition in the C4-2 xenografts.

There are limitations to our study. First, for logistic reasons, the baseline tumor size was measured 5 d before treatment in all agent groups, leading to an overestimation of tumor growth during the therapy phase. Between baseline measurement and the next measurements at days 1 and 2, tumor sizes doubled on average; therefore, taking day 0 as the reference day, tumor fold-changes would theoretically be smaller in all groups. Second, the predefined endpoint of the study at 6 wk was a bias for the comparison of survival between the 2 groups. Third, the extrapolation of preclinical data in mice to potential clinical application is difficult. Reasons include differences in PSMA homologs and expression between humans and mice, in nonspecific uptake, and in pharmacokinetics. Therefore, extrapolation of dosimetry from mice to humans is prone to several potential errors. Similar to data in the literature, our preclinical dosimetry results were lower than data reported for dosimetry conducted after clinical use. However, the main message derived from our data relies on comparison of the 2 ligands in an identical preclinical setting. Whether the differences observed in mice translate into clinical data needs to be investigated.

CONCLUSION

Our preclinical data demonstrate that the biodistribution and clearance kinetics of $^{19}F/^{177}Lu$-rhPSMA-7.3 are broadly similar to those of ^{177}Lu-PSMA I&T. However, effective doses to xenografts were substantially higher for $^{19}F/^{177}Lu$-rhPSMA-7.3 than for ^{177}Lu-PSMA I&T at equivalent doses to normal organs. This finding translated into a higher antitumor effect in a preliminary endoradiotherapy study, designating $^{19}F/^{177}Lu$-rhPSMA-7.3 an interesting candidate for clinical translation. However, future clinical trials evaluating $^{19}F/^{177}Lu$-rhPSMA-7.3 need to investigate whether the favorable preclinical profile translates into enhanced clinical antitumor effect without additional safety concerns.

DISCLOSURE

There is a patent application for rhPSMA (Hans-Jürgen Wester, Alexander Wurzer, and Matthias Eiber). Hans-Jürgen Wester and Matthias Eiber received funding from the Deutsche Forschungsgemeinschaft (Sonderforschungsbereich 824, Project B11) and Blue Earth Diagnostics Ltd. (licensee for rhPSMA) as part of an academic collaboration. Hans-Jürgen Wester is founder, shareholder, and advisory board member of Scintomics GmbH, Fuerstenfeldbruck, Germany. Matthias Eiber and Wolfgang Weber are consultants for Blue Earth Diagnostics Ltd. No other potential conflict of interest relevant to this article was reported.

ACKNOWLEDGMENTS

We thank Sybille Reder, Markus Mittelhäuser, Sandra Sühnel, Hannes Rolbieski, Birgit Blechert, and Martin Grashei for technical support in the studies.

KEY POINTS

QUESTION: Are biodistribution, dosimetry, and therapeutic efficacy comparable between $^{19}F/^{177}Lu$-rhPSMA-7.3 and ^{177}Lu-PSMA I&T?

PERTINENT FINDINGS: In preclinical prostate cancer xenograft models, uptake of $^{19}F/^{177}Lu$-rhPSMA-7.3 was, mainly, initially higher than that of ^{177}Lu-PSMA I&T, with a faster clearance profile resulting in lower absorbed doses. $^{19}F/^{177}Lu$-rhPSMA-7.3 showed higher tumor uptake and significantly better therapeutic efficacy.

IMPLICATIONS FOR PATIENT CARE: The preclinical data indicating that $^{19}F/^{177}Lu$-rhPSMA-7.3 has a better profile for radioligand treatment has to be explored in prospective clinical studies.

REFERENCES

1. von Eyben FE, Picchio M, von Eyben R, Rhee H, Bauman G. ^{68}Ga-labeled prostate-specific membrane antigen ligand positron emission tomography/computed tomography for prostate cancer: a systematic review and meta-analysis. *Eur Urol Focus.* 2018;4:686–693.
2. Perera M, Papa N, Roberts M, et al. Gallium-68 prostate-specific membrane antigen positron emission tomography in advanced prostate cancer: updated diagnostic utility, sensitivity, specificity, and distribution of prostate-specific membrane antigen-avid lesions—a systematic review and meta-analysis. *Eur Urol.* 2020;77:403–417.
3. Heck MM, Tauber R, Schwaiger S, et al. Treatment outcome, toxicity, and predictive factors for radioligand therapy with ^{177}Lu-PSMA-I&T in metastatic castration-resistant prostate cancer. *Eur Urol.* 2019;75:920–926.
4. Rahbar K, Ahmadzadehfar H, Kratochwil C, et al. German multicenter study investigating ^{177}Lu-PSMA-617 radioligand therapy in advanced prostate cancer patients. *J Nucl Med.* 2017;58:85–90.
5. Seifert R, Seitzer K, Herrmann K, et al. Analysis of PSMA expression and outcome in patients with advanced prostate cancer receiving ^{177}Lu-PSMA-617 radioligand therapy. *Theranostics.* 2020;10:7812–7820.
6. Wurzer A, Di Carlo D, Schmidt A, et al. Radiohybrid ligands: a novel tracer concept exemplified by ^{18}F- or ^{68}Ga-labeled rhPSMA inhibitors. *J Nucl Med.* 2020;61:735–742.
7. Sanchez-Crespo A. Comparison of gallium-68 and fluorine-18 imaging characteristics in positron emission tomography. *Appl Radiat Isot.* 2013;76:55–62.
8. Wester HJ, Schottelius M. PSMA-targeted radiopharmaceuticals for imaging and therapy. *Semin Nucl Med.* 2019;49:302–312.
9. Oh SW, Wurzer A, Teoh EJ, et al. Quantitative and qualitative analyses of biodistribution and PET image quality of a novel radiohybrid PSMA, ^{18}F-rhPSMA-7, in patients with prostate cancer. *J Nucl Med.* 2020;61:702–709.
10. Eiber M, Kroenke M, Wurzer A, et al. ^{18}F-rhPSMA-7 PET for the detection of biochemical recurrence of prostate cancer after radical prostatectomy. *J Nucl Med.* 2020;61:696–701.
11. Kroenke M, Wurzer A, Schwamborn K, et al. Histologically confirmed diagnostic efficacy of ^{18}F-rhPSMA-7 PET for N-staging of patients with primary high-risk prostate cancer. *J Nucl Med.* 2020;61:710–715.
12. Wurzer A, Parzinger M, Konrad M, et al. Preclinical comparison of four ^{18}F-rhPSMA-7 isomers: influence of the stereoconfiguration on pharmacokinetics. *EJNMMI Res.* 2020;10:149.
13. Baum RP, Kulkarni HR, Schuchardt C, et al. Lutetium-177 PSMA radioligand therapy of metastatic castration-resistant prostate cancer: safety and efficacy. *J Nucl Med.* 2016;57:1006–1013.
14. Cunningham D, You Z. In vitro and in vivo model systems used in prostate cancer research. *J Biol Methods.* 2015;2:e17.
15. Yuan J. Estimation of variance for AUC in animal studies. *J Pharm Sci.* 1993;82:761–763.
16. Kirschner AS, Ice RD, Beierwaltes WH. Radiation dosimetry of ^{131}I-19-iodocholesterol: the pitfalls of using tissue concentration data—reply. *J Nucl Med.* 1975;16:248–249.
17. Kirschner AS, Ice RD, Beierwaltes WH. Radiation dosimetry of 131I-19-iodocholesterol: the pitfalls of using tissue concentration data—reply. *J Nucl Med.* 1975;16:248–249.
18. Stabin MG, Sparks RB, Crowe E. OLINDA/EXM: the second-generation personal computer software for internal dose assessment in nuclear medicine. *J Nucl Med.* 2005;46:1023–1027.
19. Stabin MG, Konijnenberg MW. Re-evaluation of absorbed fractions for photons and electrons in spheres of various sizes. *J Nucl Med.* 2000;41:149–160.
20. Weineisen M, Schottelius M, Simecek J, et al. ^{68}Ga- and ^{177}Lu-labeled PSMA I&T: optimization of a PSMA-targeted theranostic concept and first proof-of-concept human studies. *J Nucl Med.* 2015;56:1169–1176.
21. Chatalic KLS, Heskamp S, Konijnenberg M, et al. Towards personalized treatment of prostate cancer: PSMA I&T, a promising prostate-specific membrane antigen-targeted theranostic agent. *Theranostics.* 2016;6:849–861.
22. Schottelius M, Wirtz M, Eiber M, Maurer T, Wester HJ. [^{111}In]PSMA-I&T: expanding the spectrum of PSMA-I&T applications towards SPECT and radioguided surgery. *EJNMMI Res.* 2015;5:68.
23. Kratochwil C, Bruchertseifer F, Rathke H, et al. Targeted alpha-therapy of metastatic castration-resistant prostate cancer with ^{225}Ac-PSMA-617: swimmer-plot analysis suggests efficacy regarding duration of tumor control. *J Nucl Med.* 2018;59:795–802.
24. Langbein T, Chausse G, Baum RP. Salivary gland toxicity of PSMA radioligand therapy: relevance and preventive strategies. *J Nucl Med.* 2018;59:1172–1173.
25. Gafita A, Fendler WP, Hui W, et al. Efficacy and safety of ^{177}Lu-labeled prostate-specific membrane antigen radionuclide treatment in patients with diffuse bone marrow involvement: a multicenter retrospective study. *Eur Urol.* 2020;78:148–154.
26. Hofman MS, Violet J, Hicks RJ, et al. [^{177}Lu]-PSMA-617 radionuclide treatment in patients with metastatic castration-resistant prostate cancer (LuPSMA trial): a single-centre, single-arm, phase 2 study. *Lancet Oncol.* 2018;19:825–833.
27. Kratochwil C, Bruchertseifer F, Rathke H, et al. Targeted α-therapy of metastatic castration-resistant prostate cancer with ^{225}Ac-PSMA-617: swimmer-plot analysis suggests efficacy regarding duration of tumor control. *J Nucl Med.* 2018;59:795–802.
28. Rathke H, Kratochwil C, Hohenberger R, et al. Initial clinical experience performing sialendoscopy for salivary gland protection in patients undergoing ^{225}Ac-PSMA-617 RLT. *Eur J Nucl Med Mol Imaging.* 2019;46:139–147.
29. Schmittgen TD, Zakrajsek BA, Hill RE, et al. Expression pattern of mouse homolog of prostate-specific membrane antigen (FOLH1) in the transgenic adenocarcinoma of the mouse prostate model. *Prostate.* 2003;55:308–316.
30. Simons BW, Turtle NF, Ulmert DH, Abou DS, Thorek DLJ. PSMA expression in the Hi-Myc model; extended utility of a representative model of prostate adenocarcinoma for biological insight and as a drug discovery tool. *Prostate.* 2019;79:678–685.
31. Rupp NJ, Umbricht CA, Pizzuto DA, et al. First clinicopathologic evidence of a non-PSMA-related uptake mechanism for ^{68}Ga-PSMA-11 in salivary glands. *J Nucl Med.* 2019;60:1270–1276.
32. Tönnesmann R, Meyer PT, Eder M, Baranski AC. [^{177}Lu]Lu-PSMA-617 salivary gland uptake characterized by quantitative *in vitro* autoradiography. *Pharmaceuticals (Basel). 2019;12:18.*
33. Weineisen M, Schottelius M, Simecek J, et al. ^{68}Ga- and ^{177}Lu-labeled PSMA I&T: optimization of a PSMA-targeted theranostic concept and first proof-of-concept human studies. *J Nucl Med.* 2015;56:1169–1176.
34. Fendler WP, Reinhardt S, Ilhan H, et al. Preliminary experience with dosimetry, response and patient reported outcome after ^{177}Lu-PSMA-617 therapy for metastatic castration-resistant prostate cancer. *Oncotarget.* 2017;8:3581–3590.
35. Delker A, Fendler WP, Kratochwil C, et al. Dosimetry for ^{177}Lu-DKFZ-PSMA-617: a new radiopharmaceutical for the treatment of metastatic prostate cancer. *Eur J Nucl Med Mol Imaging.* 2016;43:42–51.
36. Kabasakal L, Toklu T, Yeyin N, et al. Lu-177-PSMA-617 prostate-specific membrane antigen inhibitor therapy in patients with castration-resistant prostate cancer: stability, bio-distribution and dosimetry. *Mol Imaging Radionucl Ther.* 2017;26:62–68.
37. Scarpa L, Buxbaum S, Kendler D, et al. The $^{68}Ga/^{177}Lu$ theragnostic concept in PSMA targeting of castration-resistant prostate cancer: correlation of SUVmax values and absorbed dose estimates. *Eur J Nucl Med Mol Imaging.* 2017;44:788–800.
38. Violet J, Jackson P, Ferdinandus J, et al. Dosimetry of ^{177}Lu-PSMA-617 in metastatic castration-resistant prostate cancer: correlations between pretherapeutic imaging and whole-body tumor dosimetry with treatment outcomes. *J Nucl Med.* 2019;60:517–523.
39. Okamoto S, Thieme A, Allmann J, et al. Radiation dosimetry for ^{177}Lu-PSMA I&T in metastatic castration-resistant prostate cancer: absorbed dose in normal organs and tumor lesions. *J Nucl Med.* 2017;58:445–450.
40. Kuo H-T, Merkens H, Zhang Z, et al. Enhancing treatment efficacy of ^{177}Lu-PSMA-617 with the conjugation of an albumin-binding motif: preclinical dosimetry and endoradiotherapy studies. *Mol Pharm.* 2018;15:5183–5191.